Melt Pool Segmentation for Additive Manufacturing: A Generative Adversarial Network Approach

Weibo Liu, Zidong Wang, Lulu Tian, Stanislao Lauria and Xiaohui Liu

Abstract

Additive manufacturing (AM) is a popular manufacturing technique which is broadly exploited in rapid prototyping and fabricating components with complex geometries. To ensure the stability of the AM process, it is of critical importance to obtain high-quality thermal images by using image processing techniques. In this paper, a novel image processing method is put forward with aim to improve the contrast ratio of the thermal images for image segmentation. To be specific, an image-enhancement generative adversarial network (IEGAN) is developed, where a new objective function is designed for the training process. To verify the superiority and feasibility of the proposed IEGAN, the thermal images captured from an AM process are utilized for image segmentation. Experiment results demonstrate that the developed IEGAN outperforms the original GAN in improving the contrast ratio of the thermal images.

Index Terms

Additive manufacturing, generative adversarial network, defect detection, image processing, image segmentation, thermal image.

I. Introduction

The past few years have witnessed the rapid development of the additive manufacturing (AM) technologies [1]. Owing to their strong capabilities of manufacturing or replacing customized components that exhibit complex geometry and structure, the AM technologies have been successfully applied to various areas which include, but are not limited to, aerospace industry, healthcare sector and automotive engineering [2]. The AM technologies enable the rapid manufacturing of metal components with complicated geometries which are difficult or even impossible to be built by using the traditional manufacturing methods, such as the high added-value components and lightweight components. It should be pointed out that the AM approaches are more efficient and cheaper than traditional manufacturing methods in numerous applications from prototypes to fabricated products with complex geometries and structures.

The directed energy deposition (DED) method is a popular AM technique, which utilizes high-power energy sources (such as laser or wire-arc) to create a *melt pool* (i.e., the region of molten metal) on the surface of a substrate where the metal powder is deposited to form the desired geometry [1]. The melt pool is highly related to the solidification of the component, which indicates that the morphology of the melt pool plays an important role in reflecting the geometric integrity, microstructure

This work was supported in part by the European Union's Horizon 2020 Research and Innovation Programme under Grant 820776 (INTEGRADDE), the National Natural Science Foundation of China (61903065), the China Postdoctoral Science Foundation (2018M643441), the Engineering and Physical Sciences Research Council (EPSRC) of the UK, the Royal Society of the UK, and the Alexander von Humboldt Foundation of Germany. (*Corresponding author: Zidong Wang*)

W. Liu, Z. Wang, S. Lauria and X. Liu are with the Department of Computer Science, Brunel University London, Uxbridge, Middlesex, UB8 3PH, United Kingdom. (email: Zidong.Wang@brunel.ac.uk)

L. Tian is with the School of Automation Engineering, University of Electronic Science and Technology of China, Sichuan 611731, China.

and mechanical properties of fabricated components [3]. Therefore, it is of practical significance to monitor the melt pool morphology in the AM processes. In general, thermal imaging cameras are employed in the DED-based AM processes to capture the thermal images of the melt pool. Recently, the investigation of the melt pool morphology has attracted enormous interests in both academic and industrial communities [4]–[8]. For example, the control problem of the melt pool size has been studied in [4] to understand the transient changes during the AM process. In [7], a self-consistent model has been developed to simulate the heat transfer and fluid flow in the melt pool during the AM process. In addition, a two-dimensional cross-sectional model has been developed in [8] to analyze the melt pool spreading issue during the laser solid forming process.

Notice that the melt pool may splash, shrink as well as elongate, and thus becomes unstable according to the complex thermal environment during the AM process. It is therefore difficult to build a satisfactory model to simulate the morphology of the melt pool [3]. It is well known that the thermal imaging system is a popular technique in measuring the melt pool dimension. For example, the infrared thermal imaging technique has been utilized in [5] for analyzing the dimension of the melt pool in the selective laser melting process. To further study the morphology of the melt pool, image segmentation methods are employed to extract the shape of the melt pool in the thermal images. The thresholding-based methods are popular image segmentation methods due to the advantages of fast processing speed and relatively small storage space. As a typical class of thresholding-based methods, the so-called bi-level thresholding-based methods partition the background and the target object according to the threshold [9]. Thus, the selection of a suitable threshold plays an essential role in image segmentation, especially when dealing with the images corrupted by the blurring effect and noise [10].

Owing to the rapid development of artificial intelligence, the popular machine learning technique seems to be an appropriate option for image segmentation so as to quantify the morphology of the melt pool [6], [11]. In [6], a spatial reconstruction methodology has been developed to analyze thermal images for process monitoring and control of the AM process. Very recently, a data-driven predictive melt pool model has been established in [11] to control the melt pool variation for the laser powder bed fusion AM process.

Served as a powerful family of machine learning techniques, the deep learning techniques have been successfully applied to a variety of research areas, such as image processing, signal processing, telecommunication and so on. Particularly, the deep leaning techniques have been widely exploited in image segmentation owing to their strong ability in feature extraction [12]. Although deep learning algorithms have proven to be effective in dealing with image segmentation tasks, there are still some challenging problems to be considered: 1) the deep leaning techniques require “effective data” for the model training; and 2) the data collection is expensive and time-consuming.

To tackle the above-mentioned challenges, the generative adversarial network (GAN) seems to be a proper candidate due to its strong abilities in data generation and feature extraction [13]. In recent years, the GANs have been extensively applied to a great variety of real-world applications, and some representative examples include data generation, image in-painting, image translation, image synthesis, and image super-resolution [14]. It is worth mentioning that GANs have been successfully exploited in image translation of thermal images thanks to their strong learning and pattern recognition abilities. Motivated by the above discussions, we endeavor to put forward a GAN-based image processing approach for segmenting the thermal images obtained during an AM process. In this regard, a target-driven model is developed by designing a new objective function for training the GAN, which has the capability of improving the contrast ratio of the input images.

To sum up, the purpose of this paper is to develop a GAN-based image processing method with hope to segment the thermal images and extract the shape of the melt pool. The contributions of this paper can be outlined as follows: 1) an image enhancement GAN (IEGAN) is developed and utilized for segmenting the thermal images captured from an AM process for the first time; 2) a novel objective function of the IEGAN is designed with the purpose of improving the contrast ratio of the image; and 3) the performance of the IEGAN algorithm is comprehensively evaluated and employed in thermal imaging

analysis. Experiment results show that the IEGAN outperforms the original GAN, thereby benefiting the feature extraction. By using the IEGAN-based image processing method to analyze the thermal images, the shape of the melt pool is extracted, which would help quantify and characterize the morphology of melt pool.

The remaining part of this paper is organized as follows. Section II describes the background of the AM process, the DED technologies and thermal imaging analysis. In Section III, the basic knowledge of the original GAN is provided, and the proposed IEGAN is introduced with details. In Section IV, data pre-processing, experiment results and discussions are outlined. Finally, conclusions are drawn and future research topics are presented in Section V.

II. Background

With the purpose of fabricating certified components with satisfactory quality, it is of vital importance to implement the online monitoring of the welding process. Normally, the thermal cameras are used to monitor the welding process during a DED-based AM process. In this context, the morphology of the melt pool is investigated by segmenting the acquired thermal images. In this section, we first review the background of the AM process and the DED technology. Then, we discuss the online monitoring of the welding process by using the thermal imaging cameras.

A. AM Process and DED Technologies

During the past few decades, the AM processes have received an ever-increasing interest from various communities, such as manufacturing, electrical engineering, medical science, and so on [2], [7]. The AM processes have been successfully applied to produce components with complex geometries and structures. Among the AM processes, the DED technologies have been widely utilized in producing customized components and repairing components with complex structures [1]. Notice that a variety of complicated phenomena, e.g., thermal conduction, the absorption of the laser radiation in the substrate, and the solidification of the melt pool, would occur in the DED process [2].

The components fabricated by using the DED-based AM processes have the problem of poor quality, which indicates that the components are likely to have cracks, porosity, layer delamination and other defects [15]. In this context, there is a fundamental need to guarantee the quality and repeatability of the fabricated components, especially for industries that require certification constraints, such as aerospace, instrument engineering, and medical. Generally, the process monitoring is implemented to enhance the stability and robustness of the AM processes. Moreover, the process data analysis is employed to detect the defects and predict the process errors. In recent years, a vast body of work has been presented to develop online monitoring and defect detection methods [2].

B. Thermal Imaging Analysis

Nowadays, the thermal imaging technique has been extensively exploited in quality monitoring and non-destructive testing thanks to the rapid development of computer science, imaging, electrical and electronic techniques [16]. The thermal imaging technique has proven to be effective in studying the thermal properties of the target. It is worth pointing out that the DED technologies require relatively high energy to melt and fuse the metal powder material on the substrate. A challenging problem of the AM process by using the DED technologies is to avoid the melt pool instability which may be caused by the material spattering and the material evaporation from the melted area [11], [15]. To overcome the melt pool instability problem, the online monitoring of the melt pool by using the thermal imaging cameras has been exploited as a quality measurement method to ensure the stability of the AM process and produce certified components.

Note that the geometry of the melt pool has been recognized as an important quality measure. As such, the morphology (e.g. shape and size) of the melt pool has been widely investigated so as to determine the surface roughness and other defects

of the fabricated components. The infrared thermal imaging cameras are normally utilized to quantitatively investigate the morphology of the melt pool and observe the spattering phenomenon [2]. Each thermal image reflects the temperature of the melt pool area. The shapes of the melt pool are different due to the complex heat environment. Hence, it is almost impossible to manually categorize the melt pool images with satisfactory accuracy. A potential solution is to apply the machine learning techniques for feature extraction and image segmentation of the melt pool. In this paper, a GAN-based image processing method is established to improve the contrast ratio of the acquired thermal images for image segmentation.

III. Generative Adversarial Networks

In this section, the background of the GAN is presented, and the development of various GANs is reviewed. To detect the melt pool in the thermal images, an IEGAN is put forward where a penalty term is added in the objective function with hope to enhance the contrast ratio of the image. Both frameworks of the original GAN and the developed IEGAN are provided.

A. Development of GANs

In the past few years, the GAN has become one of the most popular deep learning techniques in the computer science and manufacturing societies. Owing to their distinctive merits in data generation and feature extraction, the GANs have been successfully applied to computer vision, industrial maintenance, image processing, and speech recognition.

A GAN is composed of two networks, which are the generative network, and the discriminative network [13]. The generative network as well as the discriminative network are also called as the generator and the discriminator, respectively. It is worth pointing out that both the generator and the discriminator are trained in an adversarial learning manner.

The training process of the original GAN is to train a discriminator and a generator simultaneously. Notice that the purpose of the discriminator is to distinguish between real samples and generated *fake* samples. The generator tries to generate fake samples *as real as possible* to "cheat" the discriminator. The framework of the original GAN is depicted in Fig. 1.

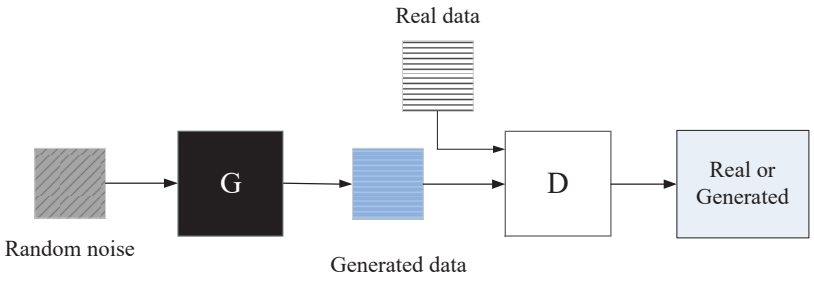

Fig. 1. The architecture of the original GAN (G is the generator; D is the discriminator)

So far, tremendous efforts have been devoted to developing various GANs with hope to improve the generalization performance of the original GAN [13], [14], [17]–[20]. The GAN variants can be briefly categorized into the following two aspects: 1) GANs with modified network architectures; and 2) GANs with task-oriented objective functions.

Up to now, some GANs have been focused on modifying the network architecture, for example, the deep convolutional GAN has been proposed in [19] by employing the convolutional neural networks (CNNs) as the generator and the discriminator. Unfortunately, a traditional CNN has the limitation that it can only capture the local spatial information, and this leads to the difficulty in dealing with multi-class images. To overcome this difficulty, the self-attention GAN has been introduced in [20] by utilizing an attention-driven framework for image generation. It is worth mentioning that the stacked GAN has been put forward in [14] where a series of GANs have been stacked in a top-down manner. The stacked GAN demonstrates that the quality of the generated images is much better than that of the original GAN.

On the other hand, an ever-increasing research interest has been attracted to design new loss functions of the GANs in order to improve the stability during the learning process. For instance, the mode regularized GAN has been put forward where a metric regularization has been introduced to penalize missing modes, which has been employed to solve the mode collapse problem [18]. The least squares GAN has been proposed where the least squares loss function has been designed for the discriminator to remedy the vanishing gradients problem during the training process [13]. In addition, the Wasserstein GAN has been introduced in [17] where the Wasserstein distance has been used to design the loss function. The Wasserstein GAN improves the learning stability by comparing with the original GAN.

B. The Structure of the IEGAN

In this paper, we aim to put forward a novel IEGAN with application in thermal imaging analysis. To achieve the target of detecting the melt pool in the thermal images, the developed IEGAN is exploited for image segmentation. It should be noted that the proposed IEGAN is a variant of the original GAN, which focuses on the design of new objective function. To be specific, a penalty term is introduced in the designed objective function to improve the contrast ratio of the thermal image for image segmentation.

The network architecture of the IEGAN is the same as the original GAN. The IEGAN consists of one generator and one discriminator. The architecture of the IEGAN is shown in Fig. 2.

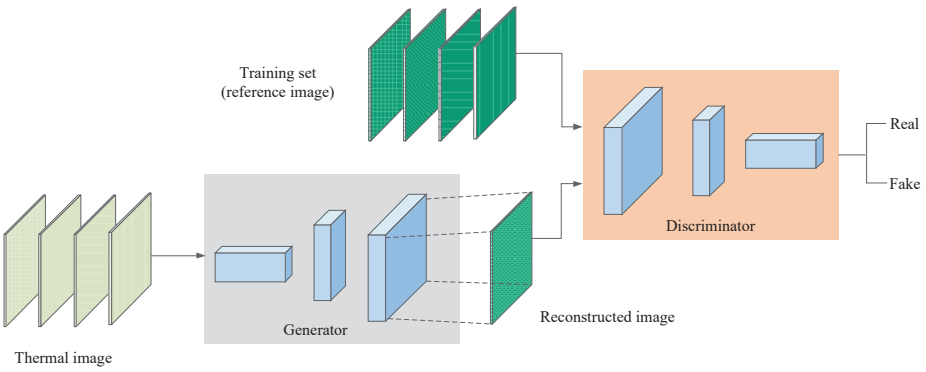

Fig. 2. The architecture of the IEGAN

Notice that the purpose of the generator in the IEGAN is to generate “high quality” images which are the improved thermal images with an enhanced contrast ratio. Different from the original GAN, the input of the generator in the IEGAN is the thermal image (raw data captured by the thermal imaging camera). The output of the generator is the improved thermal image. The discriminator aims to distinguish the generated image and the real image. In this paper, the real image is also called as the reference image, which is the pre-processed thermal image by using the pre-processing method proposed in [21].

C. The Objective Function of the IEGAN

In the original GAN, the optimization of the generator and the discriminator for an image processing task is a two-player minimax game with the following objective function:

$$\begin{aligned}\min_G \max_D J(G,D) = \mathbb{E}_{x\sim\mathbb{P}_{\text{real}}(x)}[\log D(x)] \\ + \mathbb{E}_{z\sim\mathbb{P}_z(z)}[\log(1-D(G(z)))]\end{aligned} \tag{1}$$

where x represents the reference image; z is the raw image; $G(z)$ is the output image of the generator; $D(\cdot)$ stands for the output of the discriminator; $\mathbb{P}_{\text{real}}$ and $\mathbb{P}_z$ represent the distribution of the pixel values in the reference image and that in the raw image, respectively.

In our work, we aim to improve the contrast ratio of the thermal images to further extract the shape of the melt pool through the DED process. In this context, a penalty term is introduced in the objective function of the IEGAN for image enhancement. The objective function of the IEGAN is shown in Eq. (2):

$$J_{\mathrm{IEGAN}}(G, D) = J(G, D) + J_{\mathrm{penalty}}(G) \tag{2}$$

where $J(G, D)$ is the objective function of the original GAN which is provided in Eq. (2), $J_{\mathrm{penalty}}(G)$ is the penalty term shown in Eq. (3).

To facilitate the requirement of image enhancement, a penalty term $J_{\mathrm{penalty}}(G)$ is introduced in Eq. (3):

$$J_{\mathrm{penalty}}(G) = \lambda \exp^{\alpha|G(z)-z|} \tag{3}$$

where λ and α denote the penalty factors which are two manually selected constant values according to experience; z is the thermal image; $G(z)$ represents the output image of the generator.

Intuitively, the penalty term is designed to improve the contrast ratio of the image, which should have the properties of monotonically increasing and differentiable. The first property could enlarge the difference between the generated image and the raw image, which benefits the binarization process for image segmentation. Therefore, a monotonically increasing function is a suitable choice. The second property is determined according to the utilization of the stochastic gradient descent optimization algorithm for training the GAN. Motivated by the above discussions, the exponential function is an appropriate choice due to its characteristics: 1) the exponential function is monotonically increasing; and 2) the exponential function is differentiable and smooth.

Remark 1: A practical problem is to choose suitable values of the penalty factors (λ and α). λ is an intensity factor that limits the penalty term. α is the parameter which represents the steepness of the curve. Both λ and α are selected according to experimental experience.

D. The Training Procedure of the IEGAN

In our work, the data pre-processing process is implemented to provide the data set, which is presented in the next section. Here, we discuss about the training process of the IEGAN algorithm, which is demonstrated in Algorithm 1. It should be noticed that the input of the generator is the raw image captured by the thermal camera. The input of the discriminator is composed of the output of the generator and the corresponding reference image (i.e. the pre-processed raw image). One thermal image and its pre-processed image form a pair of data. Detailed information of the data utilized in this paper is presented in Sec. IV.

IV. Experiment Results and Discussions

In this section, the proposed IEGAN is applied to deal with the thermal images captured through the welding process by using the DED-based AM technology. The background information of the thermal images and the data pre-processing process are discussed. The performance of the IEGAN is evaluated by comparing with the original GAN. All the experiments are conducted by using MATLAB software with the version of $2015b$ on a PC with the Intel Core $i7-4590$ 3.30 GHz CPU. The operating system of the PC is Microsoft Windows 10.

A. Thermal Images

The data is collected during an AM process by using the DED approach where the thermal imaging camera is implemented to monitor the welding process. The data set includes 24977 thermal images. The dimension of each image is a 128×128 matrix. Here, eight thermal images obtained through the welding process are displayed in Fig. 3.

Algorithm 1 Training Process of the IEGAN Algorithm

Require: Set up the mini-batch size m, the maximum number of epoch k, the penalty factors λ and α.

Require: Initialize the weights of the networks θ_g and θ_d.

for epoch number = $1 : k$ **do**

Randomly select m raw images $\{z^1, \cdots, z^m\}$ from the raw image dataset.

Select m corresponding reference images $\{x^1, \cdots, x^m\}$ from the pre-processed dataset.

Update the discriminator by ascending the stochastic gradient:

$\nabla_{\theta_d} \frac{1}{m} \sum_{i=1}^{m} \Big[\log D(x^i) + \log(1 - D(G(z^i))) \Big]$.

Select m raw images $\{z^1, \cdots, z^m\}$ from the raw image dataset.

Update the generator by descending the stochastic gradient:

$\nabla_{\theta_g} \frac{1}{m} \sum_{i=1}^{m} \Big[\log(1 - D(G(z^i))) + \lambda \exp^{\alpha |G(z^i) - z^i|} \Big]$.

end for

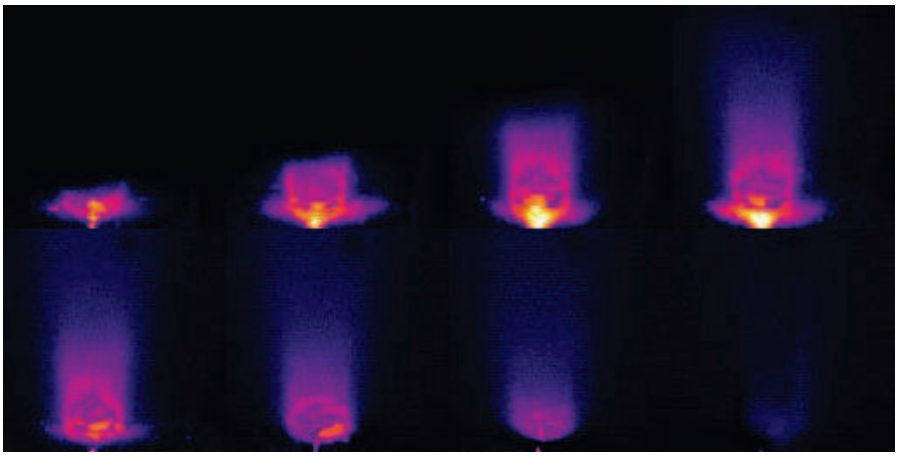

Fig. 3. Thermal images obtained through the welding process

The acquired thermal images contain three parts, namely, the background, the melt pool and the tail. Detailed information of the melt pool can be seen in [2]–[6]. The characteristic of the thermal images is different from the optical images. In the thermal images, the intensity of the pixel value reflects the temperature of that pixel. Normally, the larger the pixel value, the higher the temperature at that point. The difference between the pixel value of the current melting points and that of the nearby points is not large, which indicates that it is difficult to find an appropriate threshold to further segment the melt pool.

B. Data Pre-processing

In this paper, data pre-processing is required to produce data with *high quality* and guarantee the training performance of the GANs. The acquired thermal image is transferred to the gray image because the color does not contain much more information than the gray image. The thermal images used for training and testing the GANs are shown in Fig. 4. It should be mentioned that the pixel value of the gray image is in the range of $[0, 255]$.

Note that the training dataset of the discriminator includes the raw thermal image and its corresponding reference image. In the experiment, an automatic image processing algorithm, the so-called average threshold scanning (ATS) algorithm, developed in [21] is utilized to pre-process the thermal image, and the output image is the corresponding reference image of the thermal image. The advantages of the ATS algorithm can be summarised into three aspects: 1) easy implementation; 2) low memory requirement; and 3) relatively fast computation speed.

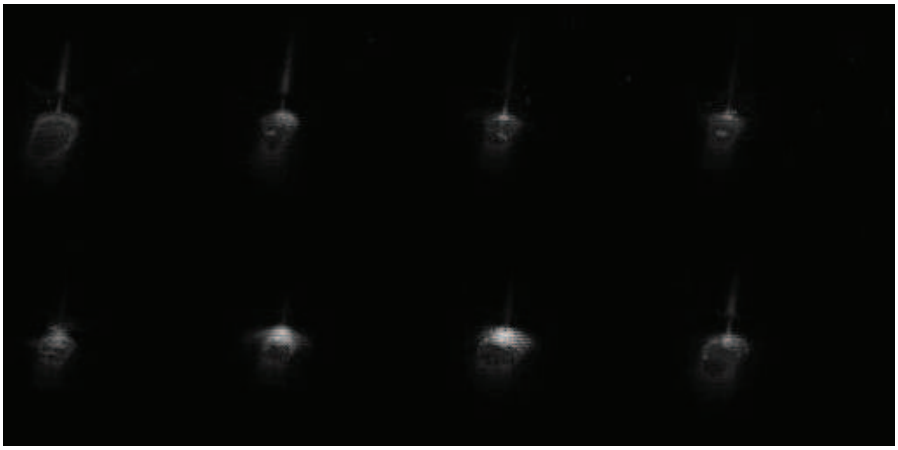

Fig. 4. Thermal images used in the experiment

To overcome the data imbalance problem, data augmentation is employed in the training process of the GANs. To be specific, the mirroring and flipping methods are used to provide effective training data. As such, a large number of effective training images and their corresponding reference images (also known as the real images) are generated.

C. Parameter Setting

In the experiment, 479 images captured at the beginning and ending stages of the AM process are removed from the database due to low image quality. 22000 images are randomly selected from the rest 24000 thermal images as the database. In the experiment, 11000 images are randomly chosen from the database as the testing dataset to evaluate the performance of the GANs. Data augmentation is employed to the other 11000 images so as to improve the diversity of data. After data augmentation, the total number of images that are used for training is 44000. All the pixel values of the thermal images used in the training and testing processes are normalized in the range of $[0, 1]$. The "Leaky ReLU" function is selected as the activation function for both the GAN and the IEGAN. The parameter settings of the networks are given in Table I.

TABLE I
CONFIGURATION OF THE IEGAN AND THE ORIGINAL GAN

Parameter	GAN	IEGAN
Learning rate	0.001	0.001
Mini-batch size	100	100
Maximum Epoch	200	30
Generator: Number of hidden layers	6	6
Generator: Number of units in each hidden layer	[100 80 64 128 640 100]	[100 80 64 128 640 100]
Discriminator: Number of hidden layers	2	2
Discriminator: Number of units in each hidden layer	[100 110]	[100 110]

The contrast improvement index (CII) is utilized as the indicator to evaluate the performance of the proposed IEGAN. CII is calculated as follows:

$$CII = \frac{C_{new}}{C_{raw}} \tag{4}$$

where C_{new} is the contrast ratio of the melt pool in the new image generated by the GANs; C_{raw} represents the contrast ratio of the raw image. The contrast ratio C of the melt pool is defined by:

$$C = \frac{I_a - I_b}{I_a + I_b} \tag{5}$$

where I_a and I_b denote the mean gray-level values of the foreground and that of the background, respectively.

D. Results

In the experiment, the thermal images are pre-processed to obtain the reference images. It should be noted that the performance of the discriminator must be better than the performance of the generator so as to guarantee the effectiveness of the training process. In this case, the discriminator is trained first in the experiment. The procedure of the developed IEGAN-based image processing method is given in Fig. 5.

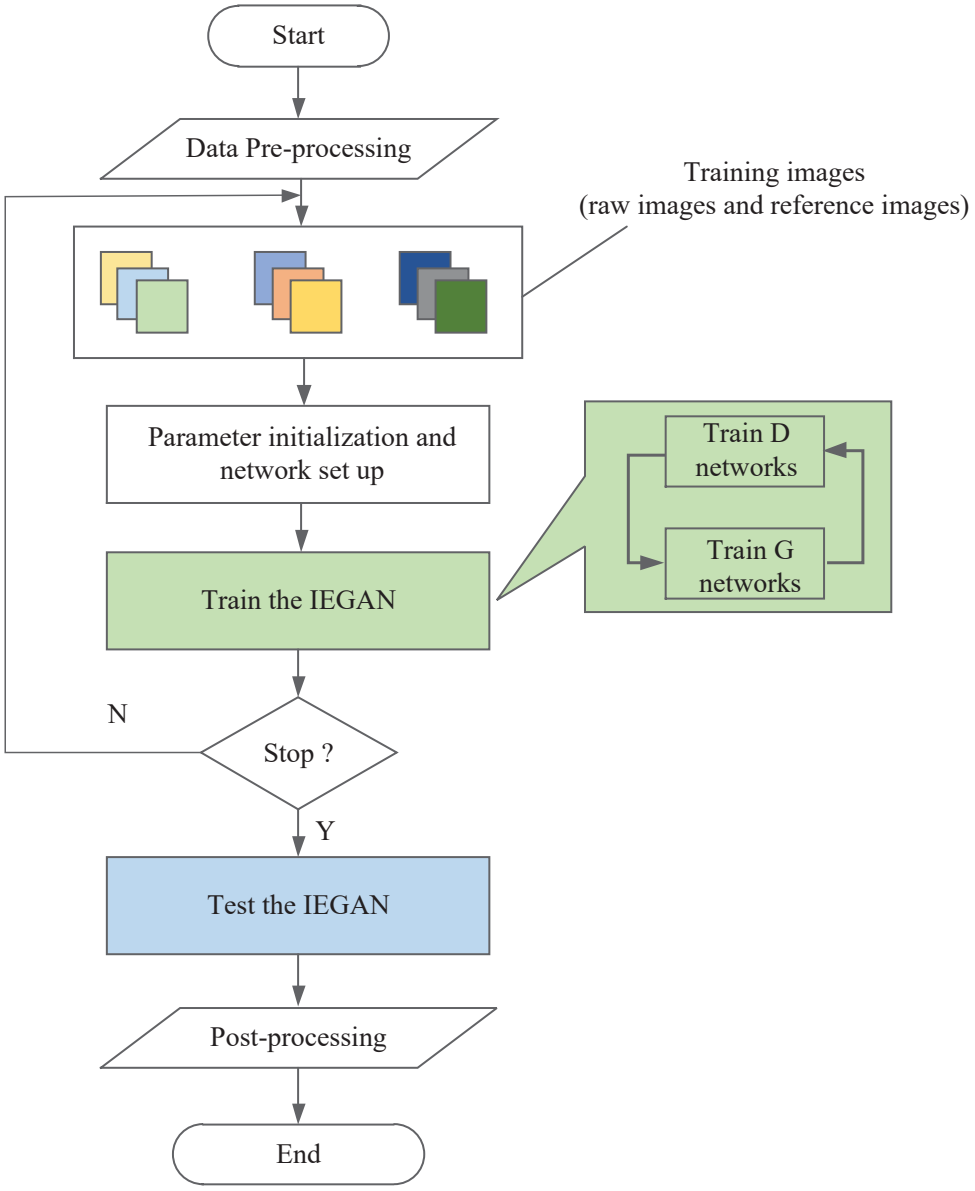

Fig. 5. Flowchart of the GAN-based image processing framework

The training curves of the original GAN and the IEGAN are depicted in Fig. 6 and Fig. 7, respectively. It can be seen in Fig. 6 that the training error of the original GAN is getting larger as the epoch increases. Additionally, the training curve of the original GAN does not converge. In Fig. 7, the training curve converges to a relatively small point, which demonstrates the superiority of the proposed IEGAN over the original GAN.

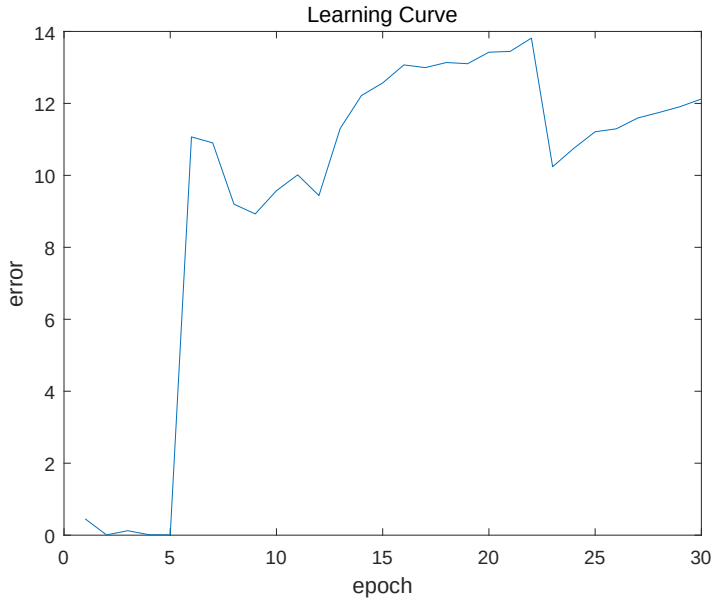

Fig. 6. Training curve of the original GAN

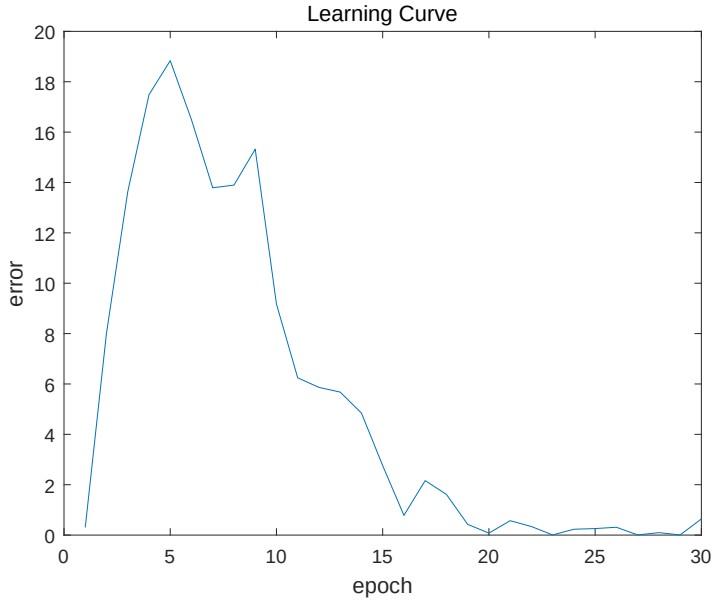

Fig. 7. Training curve of the IEGAN

The results of the original GAN are displayed in Fig. 8. It can be seen that there exists a large amount of noise in the reconstructed image. We can see that the generated image cannot reconstruct the raw input, and the shape of the melt pool cannot be accurately segmented after the binalization process. In addition, the number of epoch in training the original GAN is 200 which is much more than that of the developed IEGAN.

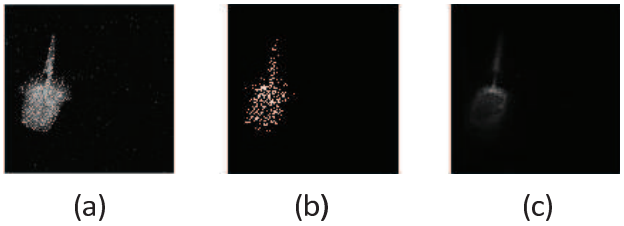

Fig. 8. Reconstructed image by using the original GAN (a) reconstructed image; (b) post-processing of (a) with the threshold of 0.6; (c) raw input

TABLE II
PERFORMANCE EVALUATION

Methods	CII
Original GAN	0.9143
IEGAN	1.1429

Experiment results of the IEGAN are shown in Figs. 9-12. We can see that the developed IEGAN demonstrates satisfactory performance in reconstructing the thermal images with an improved contrast ratio. In the experiment, the post-processing technique is employed to binarize the grayscale image with hope to extract the shape of the melt pool.

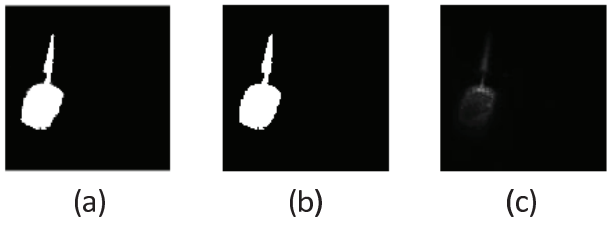

Fig. 9. Example 1: Reconstructed image by using the IEGAN (a) reconstructed image; (b) post-processing of (a) with the threshold of 0.6; (c) raw input

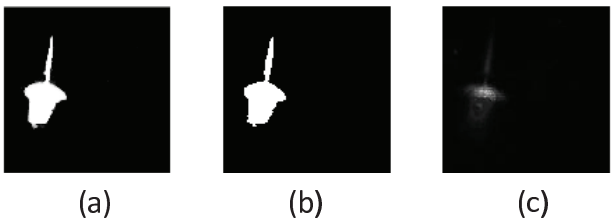

Fig. 10. Example 2: Reconstructed image by using the IEGAN (a) reconstructed image; (b) post-processing of (a) with the threshold of 0.6; (c) raw input

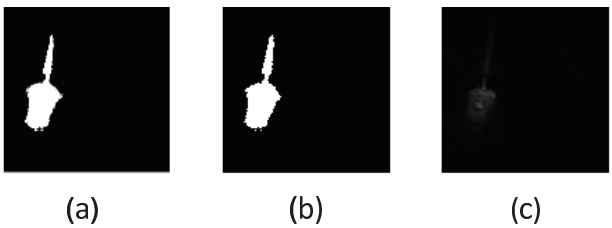

Fig. 11. Example 3: Reconstructed images by using the IEGAN (a) reconstructed image; (b) post-processing of (a) with the threshold of 0.6; (c) raw input

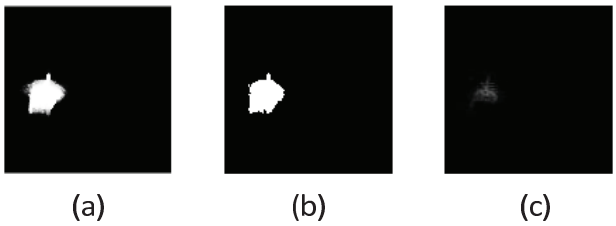

Fig. 12. Example 4: Reconstructed image by using the IEGAN (a) reconstructed image; (b) post-processing of (a) with the threshold of 0.6; (c) raw input

The CII of the original GAN and the IEGAN are shown in Table II. It can be seen that the IEGAN has a larger value of CII than the original GAN, which indicates that the image generated by the IEGAN has a higher contrast ratio than the raw image. It is clear that the IEGAN is capable of improving the contrast ratio of the input images, which can be easily used for image segmentation with a constant threshold. Note that both the reconstructed image and the post-processed image are quite "clean", which indicates that noise is reduced by using the proposed IEGAN. Thus, the superiority and feasibility of the developed IEGAN-based image processing method are demonstrated, and the shape of the melt pool is extracted which contributes to the monitoring of the AM processes.

It should be pointed out that the performance of the IEGAN is highly related to the hyperparameters (such as the learning rate, the penalty term and number of hidden layers). Owing to their strong abilities in finding satisfactory solutions in optimization problems, evolutionary computation seem to be a suitable method for choosing hyperparameters of GANs [22]–[24]. Another research topic is to apply the GAN-based algorithms in other complex systems [25]–[28].

V. Conclusion

The monitoring of the AM process plays a significant role in fabricating certified products. The states of the melting process are justified by analyzing the thermal images obtained from the thermal imaging cameras. In this paper, a new image processing method has been put forward with hope to improve the quality of the thermal images for feature extraction. To extract the shape of the melt pool, a novel IEGAN has been developed where a modified objective function has been introduced for the training process. In particular, a designed penalty term has been put forward in the objective function of the IEGAN to enhance the contrast ratio of the image reconstructed by the IEGAN. The IEGAN-based image processing method has been successfully employed to improve the quality of the thermal images captured through the DED-based AM process. The effectiveness of the proposed IEGAN has been shown by comparing the contrast ratio of the reconstructed thermal image with that of the original GAN. Experiment results have demonstrated that the proposed IEGAN outperforms the original GAN in terms of the CII. Furthermore, the shape of the melt pool has been successfully extracted on the post-processed image, which contributes to the process monitoring of the AM process. In the future, we aim to 1) improve the objective function of the IEGAN to overcome the model collapse problem; 2) introduce evolutionary computation algorithms to automatically select suitable parameters of the developed image processing framework; and 3) apply the proposed IEGAN-based image processing framework to other applications, such as thermal-to-visible image translation.

References

[1] M. Soshi, K. Odum, and G. Li, Investigation of novel trochoidal toolpath strategies for productive and efficient directed energy deposition processes, *CIRP Annals - Manufacturing Technology*, vol. 68, no. 1, pp. 241-244, 2019.

[2] L. E. Criales, Y. M. Arısoy, B. Lane, S. Moylan, A. Donmez, and T. Ozel, Laser powder bed fusion of nickel alloy 625: experimental investigations of effects of process parameters on melt pool size and shape with spatter analysis, *International Journal of Machine Tools and Manufacture*, vol. 121, pp. 22-36, 2017.

[3] M. Khanzadeh, L. Bian, N. Shamsaei, and S. M. Thompson, Porosity detection of laser based additive manufacturing using melt pool morphology clustering, In: *Proceedings of the Solid Freeform Fabrication Symposium*, Texas, USA, Aug. 2016, pp. 1487-1494.

[4] A. Birnbaum, P. Aggarangsi, and J. Beuth, Process scaling and transient melt pool size control in laser-based additive manufacturing processes, In: *Proceedings of the Solid Freeform Fabrication Symposium*, Texas, USA, Aug. 2003, pp. 328-339.

[5] B. Cheng, J. Lydon, K. Cooper, V. Cole, P. Northrop, and K. Chou, Infrared thermal imaging for melt pool analysis in SLM: a feasibility investigation, *Virtual and Physical Prototyping*, vol. 13, no. 1, pp. 8-13, 2018.

[6] D. A. Kriczky, J. Irwin, E. W. Reutzel, P. Michaleris, A. R. Nassar, and J. Craig, 3D spatial reconstruction of thermal characteristics in directed energy deposition through optical thermal imaging, *Journal of Materials Processing Technology*, vol. 221, pp. 172-186, 2015.

[7] H. Qi, J. Mazumder, and H. Ki, Numerical simulation of heat transfer and fluid flow in coaxial laser cladding process for direct metal deposition, *Journal of Applied Physics*, vol. 100, no. 2, art. no: 024903, 11 pages, 2006.

[8] J. Yu, X. Lin, J. Wang, J. Chen, and W. Huang, Mechanics and energy analysis on moltenpool spreading during laser solid forming, *Applied Surface Science*, vol. 256, no. 14, pp. 4612-4620, 2010.

[9] H.-F. Ng, Automatic thresholding for defect detection, *Pattern Recognition Letters*, vol. 27, no. 14, pp. 1644-1649, 2006.

[10] H. Gao, Z. Fu, C. M. Pun, H. Hu, and R. Lan, A multi-level thresholding image segmentation based on an improved artificial bee colony algorithm, *Computers & Electrical Engineering*, vol. 70, pp. 931-938, 2018.

[11] H. Yeung, Z. Yang, and L. Yan, A meltpool prediction based scan strategy for powder bed fusion additive manufacturing, *Additive Manufacturing*, vol. 35, art. no: 101383, 8 pages, 2020.

[12] N. Zeng, H. Li, Z. Wang, W. Liu, S. Liu, F. E. Alsaadi, and X. Liu, Deep-reinforcement-learning-based images segmentation for quantitative analysis of gold immunochromatographic strip, *Neurocomputing*, doi:10.1016/j.neucom.2020.04.001.

[13] X. Mao, Q. Li, H. Xie, R. Y. Lau, Z. Wang, and S. Paul Smolley, Least squares generative adversarial networks, In: *Proceedings of the 2017 IEEE International Conference on Computer Vision*, Venice, Italy, Oct. 2017, pp. 2794-2802.

[14] H. Zhang, T. Xu, H. Li, S. Zhang, X. Wang, X. Huang, and D. N. Metaxas, Stackgan: Text to photo-realistic image synthesis with stacked generative adversarial networks, In: *Proceedings of the 2017 IEEE International Conference on Computer Vision*, Venice, Italy, Oct. 2017, pp. 5907-5915.

[15] M. Grasso and B. M. Colosimo, Process defects and in situ monitoring methods in metal powder bed fusion: a review, *Measurement Science and Technology*, vol. 28, no. 4, art. no: 044005, 25 pages, 2017.

[16] L. Zhu, Y. Chen, P. Ghamisi, and J. A. Benediktsson, Generative adversarial networks for hyperspectral image classification, *IEEE Transactions on Geoscience and Remote Sensing*, vol. 56, no. 9, pp. 5046-5063, 2018.

[17] M. Arjovsky, S. Chintala, and L. Bottou, Wasserstein generative adversarial networks, In: *Proceedings of the 34th International Conference on Machine Learning*, Sydney, Australia, Aug. 2017, vol. 70, pp. 214-223.

[18] T. Che, Y. Li, A. P. Jacob, Y. Bengio, and W. Li, Mode regularized generative adversarial networks, *Proceedings of the 2017 International Conference on Learning Representations*, Toulon, France, Apr. 2017, pp. 1-13.

[19] A. Radford, L. Metz, and S. Chintala, Unsupervised representation learning with deep convolutional generative adversarial networks, *arXiv preprint arXiv:1511.06434*, 2015.

[20] H. Zhang, I. Goodfellow, D. Metaxas, and A. Odena, Self-Attention Generative Adversarial Networks, In: *Proceedings of the 36th International Conference on Machine Learning*, Long Beach, USA, Jun. 2019, pp. 7354-7363.

[21] Y. Cheng, L. Tian, C. Yin, X. Huang, J. Cao, and L. Bai, Research on crack detection applications of improved PCNN algorithm in MOI nondestructive test method, *Neurocomputing*, vol. 277, pp. 249-259, 2018.

[22] W. Liu, Z. Wang, N. Zeng, Y. Yuan, F. E. Alsaadi, and X. Liu, A novel randomised particle swarm optimizer, *International Journal of Machine Learning and Cybernetics*, doi:10.1007/s13042-020-01186-4.

[23] M. G. Villarreal-Cervantes, J. S. Pantoja-García, A. Rodríguez-Molina, and S. E. Benitez-Garcia, Pareto optimal synthesis of eight-bar mechanism using meta-heuristic multi-objective search approaches: application to bipedal gait generation, *International Journal of Systems Science*, vol. 52, no. 4, pp. 671-693, Mar. 2021.

[24] Z. Li and Z. Ding, Time-varying multi-objective optimisation over switching graphs via fixed-time consensus algorithms, *International Journal of Systems Science*, vol. 51, no. 15, pp. 2793-2806, Aug. 2020.

[25] Z. Zhao, Z. Wang, L. Zou and J. Guo, Set-membership filtering for time-varying complex networks with uniform quantisations over randomly delayed redundant channels, *International Journal of Systems Science*, vol. 51, no. 16, pp. 3364-3377, 2020.

[26] Y. Chen, Z. Chen, Z. Chen and A. Xue, Observer-based passive control of non-homogeneous Markov jump systems with random communication delays, *International Journal of Systems Science*, vol. 51, no. 6, pp. 1133-1147, 2020.

[27] Q. Li and J. Liang, Dissipativity of the stochastic Markovian switching CVNNs with randomly occurring uncertainties and general uncertain transition rates, *International Journal of Systems Science*, vol. 51, no. 6, pp. 1102-1118, 2020.

[28] H. Tan, B. Shen, K. Peng and H. Liu, Robust recursive filtering for uncertain stochastic systems with amplify-and-forward relays, *International Journal of Systems Science*, vol. 51, no. 7, pp. 1188-1199, 2020.

Weibo Liu received the Ph.D. degree in computer science from Brunel University London, Uxbridge, U.K. His research interests include big data analysis, image processing and deep learning techniques. He serves as an Associate Editor for the Journal of Ambient Intelligence and Humanized Computing.

Zidong Wang received the Ph.D. degree in electrical engineering from Nanjing University of Science and Technology. He is a Professor of Dynamical Systems and Computing in the Department of Computer Science, Brunel University London. He serves as the Editor-in-Chief for *Neurocomputing* and *International Journal of Systems Science*. He is a Member of the Academia Europaea and a Fellow of the IEEE.

Lulu Tian received the Ph.D. degree in the School of Automation Engineering at the University of Electronic Science and Technology of China, Chengdu, China. He is currently a researcher at the University of Electronic Science and Technology of China. His current research interests include defects detecting, neural networks, structural health monitoring, and non-destructive testing.

Stanislao Lauria received the Ph.D. degree in Cybernetics from the University of Reading (UK). He is a Lecturer at Brunel University (UK). He has been research fellow at both the University of Reading and University of Plymouth (UK). He is a computer scientist with an interest in robotics, HCI, robotics and social media, AI, robotics and education, image analysis, data processing.

Xiaohui Liu received the Ph.D. degree in computer science from Heriot-Watt University, Edinburg, U.K., in 1988. He is currently a Professor of Computing at Brunel University. He leads the Intelligent Data Analysis (IDA) Group, performing interdisciplinary research involving artificial intelligence, dynamic systems, image and signal processing, and statistics, particularly for applications in biology, engineering and medicine.